



Experimental and theoretical study of critical heat flux in vertical upflow with inlet vapor void

Chirag R. Kharangate^a, Issam Mudawar^{a,*}, Mohammad M. Hasan^b

^aBoiling and Two-phase Flow Laboratory, School of Mechanical Engineering, Purdue University, 585 Purdue Mall, West Lafayette, IN 47907-2088, USA

^bNASA Glenn Research Center, 21000 Brookpark Road, Cleveland, OH 44135, USA

ARTICLE INFO

Article history:

Received 25 April 2011

Received in revised form 18 August 2011

Accepted 18 August 2011

Available online 6 October 2011

Keywords:

Flow boiling

Separated flow

Critical heat flux (CHF)

ABSTRACT

This study explores the mechanism of flow boiling critical heat flux (CHF) for FC-72 in a 2.5 mm × 5 mm vertical upflow channel that is heated along its 2.5 mm sidewall downstream of an adiabatic development section. Unlike most prior CHF studies, where the working fluid enters the channel in liquid state, the present study concerns saturated inlet conditions with finite vapor void. Temperature measurements and high-speed video imaging techniques are used to investigate the influence of the inlet vapor void on interfacial behavior at heat fluxes up to CHF as well during the CHF transient. The flow entering the heated portion of the channel consists of a thin liquid layer covering the entire perimeter surrounding a large central vapor core. Just prior to CHF, a fairly continuous wavy vapor layer begins to develop between the liquid layer covering the heated wall and the heated wall itself, resulting in a complex four-layer flow consisting of the liquid layer covering the insulated walls, the central vapor core, the now separated liquid layer adjacent to the heated wall, and the newly formed wavy vapor layer along the heated wall. This behavior is captured in a new separated control-volume-based model that facilitates the determination of axial variations of thicknesses and mean velocities of the four layers. Incorporating the results of this model in a modified form of the Interfacial Lift-off CHF Model is shown to provide fairly good predictions of CHF data for mass velocities between 185 and 1600 kg/m² s, evidenced by a mean absolute error of 24.52%.

© 2011 Elsevier Ltd. All rights reserved.

1. Introduction

The ability to predict critical heat flux (CHF) is of paramount importance to the safety of devices and systems involving boiling along heat-flux-controlled surfaces. Exceeding CHF amounts to catastrophic failure due to overheating or physical burnout. There are several methods to increasing CHF in order to broaden the permissible range of wall heat flux. They include surface augmentation and use of high mass velocities, high subcooling and short, small diameter channels [1]. Supplying the working fluid to the channel in highly subcooled state is especially beneficial because of the fluid's ability to extract a significant portion of the supplied wall energy in the form of sensible heat prior to evaporation. This explains the popularity of subcooled flow boiling in many applications demanding the removal of large heat loads concentrated in small surface areas, such as nuclear cores, radar and directed-energy laser and microwave defense electronics [1].

However, there are many flow boiling applications where a single two-phase loop is used to cool a multitude of heat dissipating

modules. One application where this configuration is being considered is thermal control onboard future space vehicles. NASA's space shuttles use a single-phase loop to cool a number of electronic and power modules. But the complexity of future space vehicles will require significant reductions in both weight and volume of all subsystems, including thermal control. To achieve this goal, emphasis is now being placed on replacing the single-phase thermal control loop with a two-phase loop to capitalize upon the orders-of-magnitude enhancement in heat transfer coefficients possible with flow boiling and condensation in a two-phase loop [1]. Here too, CHF is a crucial design parameter, compounded by the limited 'power budget' of space systems placing stringent limits on both the maximum coolant flow rate and maximum pressure drop for the loop. Another limitation of this two-phase configuration is the gradual loss of fluid subcooling for modules that are mounted in series, where downstream modules have to contend with only saturated flow boiling with a finite vapor void fraction. Determining the influence of this inlet vapor void on flow boiling CHF is the primary focus of the present study.

Past studies have identified four possible trigger mechanisms for CHF in flow boiling: *Boundary Layer Separation*, *Bubble Crowding*, *Sublayer Dryout*, and *Interfacial Lift-off*. The Boundary Layer Separation Model is based on the postulate that CHF occurs when

* Corresponding author. Tel.: +1 765 494 5705; fax: +1 765 494 0539.

E-mail address: mudawar@ecn.purdue.edu (I. Mudawar).

URL: <https://engineering.purdue.edu/BTFPL> (I. Mudawar).

obtaining analytical solutions for key flow variables. However, because it is based on the assumptions that velocities of the liquid and vapor phases are both equal and uniform across the flow channel's cross section, this model cannot predict the velocity differences between the phases known to produce the interfacial instabilities implicit in CHF models. By permitting such differences, SFMs overcome this fundamental weakness. However, SFMs require the use of empirical coefficients to achieve solution close [18–23].

An alternative approach to predicting the velocities of the vapor and liquid portions of the flow is to use the control volume method. Here, mass, momentum and energy conservation laws are applied to control volumes encompassing the liquid and vapor phases separately, and later combined for the two-phase mixture. The control volume method proved highly effective in predicting two-phase behavior for vertical separated flow along short walls [8] and long heated walls [9,10,24–27].

Unfortunately, none of the prior theoretical CHF models can tackle saturated flow boiling with a two-phase mixture at the inlet. It is therefore the primary objective of the present study to explore experimentally and theoretically saturated flow boiling CHF in vertical upflow with a finite inlet vapor void fraction. As discussed earlier, this condition is prevalent in downstream heat-dissipating modules when a number of modules are cooled in series using a single two-phase flow loop. This study is a follow-up to a recent study by the authors that addressed similar conditions for horizontal flow boiling in a rectangular channel heated along one upward-facing wall [28]. Both high-speed video imaging and photo-micrographic techniques are used to map interfacial behavior up to CHF as well as during the CHF transient. A new control-volume-based model is used to predict velocities and thicknesses of the various layers comprising the flow. These predictions are incorporated into the Interfacial Lift-off Model to predict CHF in the presence of finite inlet vapor void. The present CHF data are also compared against the predictions of popular flow boiling correlations. This study is part of a series of studies concerning the implementation of two-phase cooling in future space vehicles.

2. Experimental methods

2.1. Flow boiling module

The flow boiling module used in this study is comprised of two polycarbonate plastic (Lexan) plates that are pressed together between two outer aluminum plates with the aid of a series of bolts. As illustrated in Fig. 1(a), a 2.5 mm × 5 mm rectangular flow channel is milled into the underside of the top plastic plate. Not shown in Fig. 1(a) is a flexible Teflon cord that is inserted into a shallow o-ring groove in the upper surface of the bottom plastic plate to guard against leaks. A honeycomb insert at the channel inlet is used to straighten the flow and break up any large eddies. The heated wall is situated towards the downstream end of the channel. The channel features an entry length 106 times the hydraulic diameter to make certain that the liquid flow becomes fully developed upstream of the heated wall. The heated wall consists of a 0.56-mm-thick by 101.6-mm-long copper plate that is heated by a series of thick-film resistors. The heated wall is inserted into a rectangular groove in the flow channel's bottom plastic plate.

Fig. 1(b) depicts the various stages of assembling the heated wall. Six of 16.1-mm-long by 4.0-mm-wide 188 Ω thick-film resistors are soldered to the underside of the copper plate. The wall temperature is measured by five thermocouples inserted into shallow holes in the copper plate between the resistors. Equal resistance ensures uniform heat flux along the heated wall, with all six resistors connected in parallel and powered by a single variable

voltage transformer. As discussed in [10], the thickness of the copper heated wall must be chosen carefully to ensure accurate CHF measurement. On one hand, a very thin wall can produce CHF that is a function of wall thickness. A minimum 'asymptotic wall thickness' is required to achieve CHF that is both insensitive to wall thickness and representative of real heat exchange surfaces. On the other hand, a very large wall thickness can greatly delay the thermal response of the wall to changes in heat input. A copper thickness of 0.56 mm proved effective at exceeding the asymptotic thickness while allowing the wall to reach steady-state temperature between heat flux increments in less than 5 s. These two requirements are based on the need to employ the present flow boiling module in future parabolic flight experiments, where steady-state thermal response must be achieved within the 23 s microgravity duration of a single parabola.

2.2. Two-phase loop

Fig. 2(a) shows a schematic of the two-phase loop that is configured to condition the FC-72 working fluid to the desired pressure, flow rate and quality at the inlet to the flow boiling module. Deaeration is achieved with the aid of a detachable accessory containing a reservoir fitted with an immersion heater, and a water-cooled condenser. The deaeration is performed before performing a series of tests.

In the main loop, the FC-72 is circulated with the aid of a variable-speed magnetically coupled pump. The flow passes through a regulating valve followed by a filter, turbine flow meter, and two in-line electrical heaters, before entering the flow boiling module. The purpose of the first in-line heater is to raise liquid temperature while maintaining single-phase liquid flow. The second in-line heater causes part of the flow to evaporate in order to achieve saturated flow with the desired flow quality at the inlet to the flow boiling module. This arrangement enables the determination of flow quality at the inlet to the flow boiling module from measurements of power input to the second in-line heater and temperature and pressure measurements both upstream and downstream of the second in-line heater. A condenser is situated downstream of the flow boiling module to return the two-phase mixture to liquid state. A constant pressure point between the condenser and pump is maintained with the aid of a nitrogen-pressurized accumulator. This device compensates for any expansion or contraction of the working fluid throughout the loop with metal bellows internal to the accumulator.

2.3. Instrumentation and measurement accuracy

An array of instruments is used to measure fluid conditions and power input throughout the flow loop. Two thermocouples are inserted in the FC-72 flow just upstream and downstream of the heated wall. As indicated earlier, the temperature of the heated wall in the flow boiling module is measured by five type-K thermocouples that are inserted equidistantly into the copper wall. Pressure transducers are also connected to taps in the flow boiling module 13 mm upstream and downstream of the heated wall. A wattmeter is used to measure electrical power input to the heated-wall's thick-film resistors. The wall heat flux is determined by dividing the power input by the wetted area of the heated wall. A second wattmeter is used to measure electrical power input to the second in-line heater. Temperature and pressure at the inlet to the second in-line heater are measured with the aid of a thermocouple and a pressure transducer, respectively. The flow rate is measured by a turbine flow meter.

Accuracies of the flow rate, pressure, and heat flux measurements are estimated at 2.3%, 0.01%, and 0.2%, respectively. The fluid

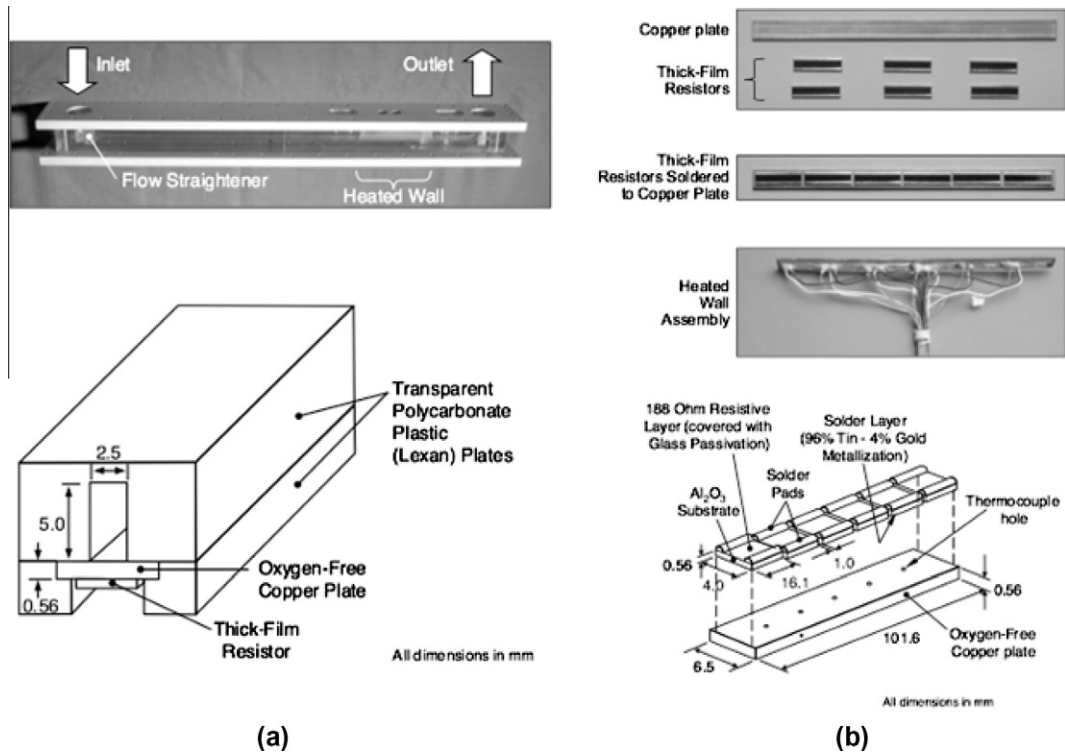


Fig. 1. (a) Flow channel assembly. (b) Construction of heated wall.

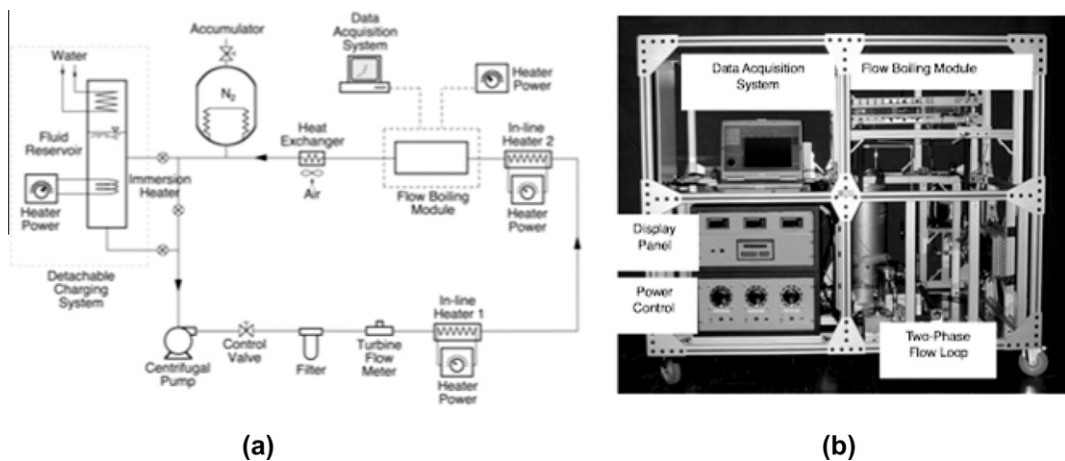


Fig. 2. (a) Schematic of two-phase loop. (b) Photo of test facility (flow boiling module is tilted into vertical upflow orientation during testing).

and wall temperatures are measured with thermocouples having an uncertainty better than 0.3 °C.

The entire apparatus, including the flow loop components, power and instrumentation cabinets and data acquisition system, is mounted onto a rigid extruded aluminum frame as shown in Fig. 2(b).

2.4. Flow visualization

A Photron Fastcam Ultima APX camera system with a shutter speed of 1/20,000 is used to capture interfacial features along the heated portion of the flow channel. High magnification is achieved with the aid of a Nikon Micro-Nikkor 105 mm f/8D autofocus lens. As shown in Fig. 3(a), the camera is positioned in a side-view orientation normal to the flow channel. The flow is backlit with a light

source, with a semi-opaque sheet placed in between to soften and diffuse the incoming light. An optical tripod allows the camera to traverse the entire vertical length of the heated wall. Optimum resolution is achieved by capturing discrete inlet, middle, and exit regions of the heated wall rather than the entire wall. Fig. 3(b) shows each of these regions spans 20 mm. Together, the three regions cover nearly 60% of the heated wall.

3. Flow visualization results

Fig. 4 shows 20 sequential video images of the inlet, middle and exit regions of the heated portion of the channel just prior to CHF (termed CHF- in the present study). The time elapsed between consecutive frames is 1.024/1024 s. Overall, there is a large central vapor core with liquid flowing near the walls. Due to the restriction

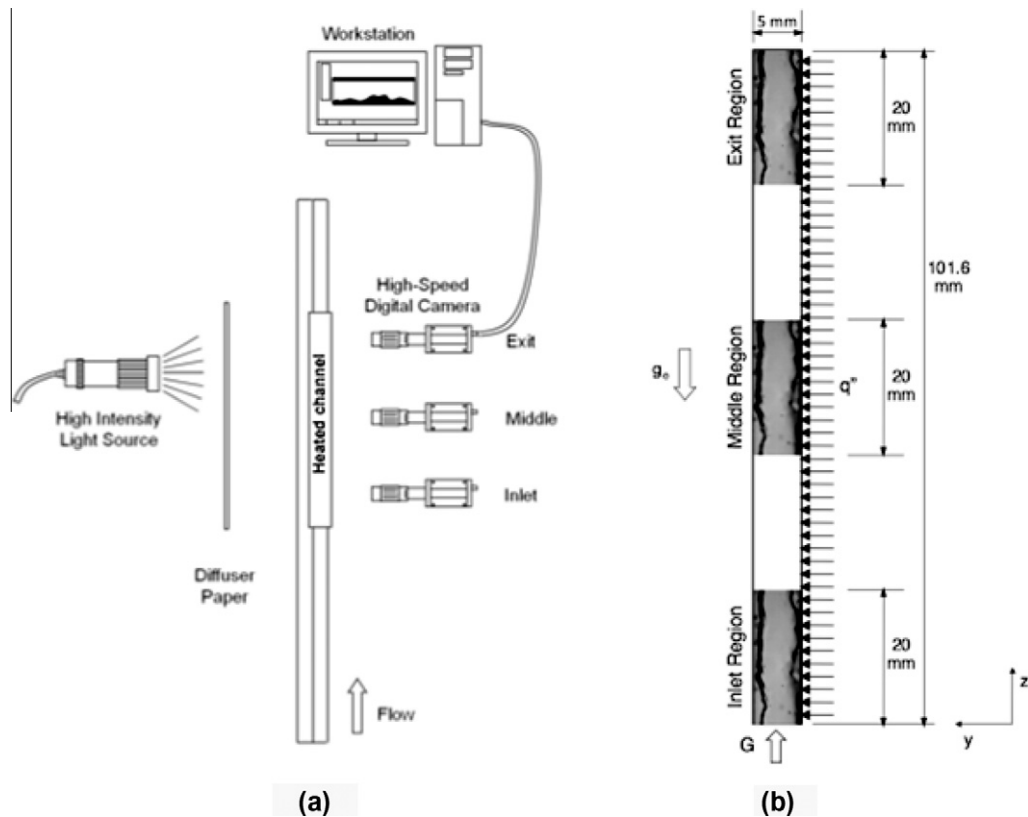


Fig. 3. (a) Flow visualization setup. (b) Inlet, middle and exit regions of heated portion of flow channel used for video capture.

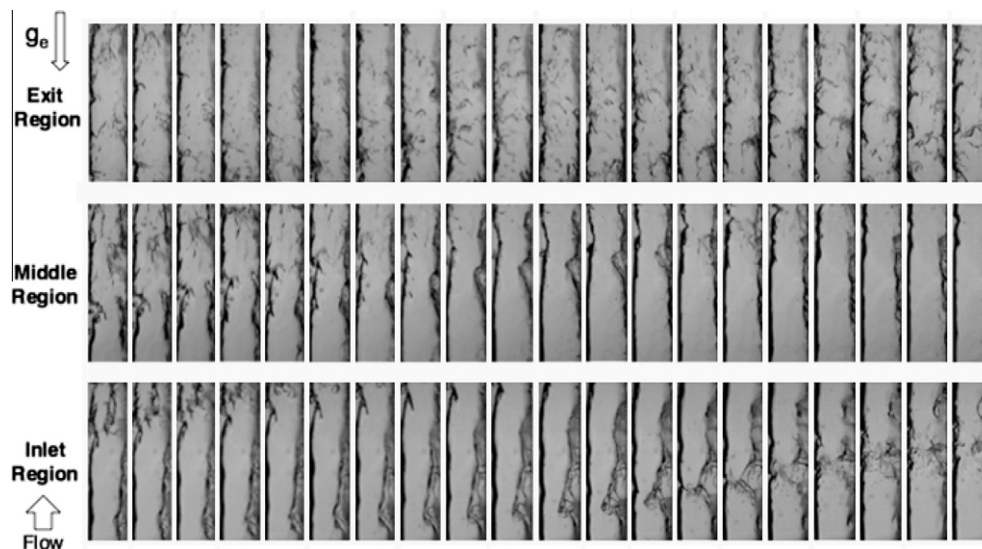


Fig. 4. Twenty sequential images of inlet, middle and exit regions of heated portion of channel captured at CHF- for $G = 340 \text{ kg/m}^2 \text{ s}$ and $x_t = 0.0127$. Heated wall is on right side of individual images.

of side viewing, it is impossible to ascertain the presence of liquid on the walls normal to the viewing direction, especially in the middle and exit regions. In the inlet region, there is a wavy vapor layer developing along the heated wall between a thin liquid layer and the heated wall. This vapor layer forms immediately at the leading edge of the heated wall. Image sequences captured at different times show temporal variations in the vapor layer's shape and thickness due to interfacial waviness. Cooling of the wall and vapor production both appear to be sustained by remnants of liquid

within or beneath the vapor layer. A thin wavy liquid layer appears to propagate along the opposite non-heated wall.

Formation of the wavy vapor layer along the heated wall resembles behavior observed in prior studies by Galloway and Mudawar [7,8], Gersey and Mudawar [24,25], Sturgis and Mudawar [26,27] and Zhang et al. [9]. Unlike the present study, the flow in all these earlier studies entered the heated portion of the channel in liquid state, but the wavy vapor layer also commenced near the upstream edge of the heated wall. In the present vertical channel, the

presence of a large vapor core at the inlet to the heated portion of the channel caused a similar behavior to be confined to the vicinity of the heated wall. Similarities of near-wall wavy vapor layer behavior between the present and earlier studies suggests that the Interfacial Lift-off mechanism proposed by Galloway and Mudawar [7,8] and later by Zhang et al. [15] as the trigger mechanism for CHF for subcooled inlet flow may be equally valid for the present high inlet vapor void configuration.

Fig. 4 shows the near-wall wavy vapor layer behavior continues in the middle and exit regions, albeit with noticeable thinning along the flow direction. This thinning may be explained by the axial flow acceleration causing substantial increases in shear stresses between the different flow layers.

Fig. 5(a) and (b) depicts the flow development for the inlet region with increasing heat flux up to 95% CHF for two different mass velocities. In the absence of heat input, there is symmetry in flow behavior along the heated right wall and non-heated left wall, which is manifest by relatively thin liquid layers at the walls separated by a large middle vapor core. Notice the marked increase in interfacial waviness between the two liquid layers and vapor core with increasing mass velocity. At 50% CHF, bubbles appear to form within the liquid layer covering the heated wall for both mass velocities, with the higher mass velocity precipitating an increase in interfacial waviness. At 95% CHF (or CHF-), there are signs of vapor bubbles coalescing into a fairly continuous wavy vapor layer between the right liquid layer and the heated wall.

Fig. 6(a) and (b) shows, for two mass velocities, the flow behavior in the inlet, middle and exit regions at 95% CHF. As discussed earlier, the most obvious change between the three regions for each mass velocity is the axial thinning of both the liquid/vapor layers along the right heated wall and the liquid layer along the left non-heated wall. The thicknesses of these layers are further reduced for the higher mass velocity case.

Fig. 7(a) and (b) shows images of the flow at CHF- and during the CHF transient (while wall temperatures begin to increase unsteadily) for $G = 340 \text{ kg/m}^2 \text{ s}$ in the inlet region and $G = 664 \text{ kg/m}^2 \text{ s}$ in the exit region, respectively. For the lower mass velocity, the layer along the heated right wall appears to disappear altogether as any liquid in this layer is vaporized. This also appears

to influence the liquid layer along the opposite non-heated left wall, which is now thinned further by the increase in core vapor velocity between CHF- and the CHF transient. It is important to note (as will be discussed later) that CHF commences first in the inlet region for the lower mass velocity case, and the exit region for the higher mass velocity. This proves that the behavior depicted in Fig. 7(a) for the lower mass velocity is a true depiction of CHF occurrence. Because of higher velocities and higher shear stresses, and occurrence of CHF in the exit region for the higher mass velocity case, Fig. 7(b), is more difficult to interpret.

4. Experimental results

Fig. 8 shows boiling curves measured by the heated wall's thermocouple where CHF commenced first for $G = 343, 970$ and $1589 \text{ kg/m}^2 \text{ s}$. The heat flux is plotted against the difference between wall and saturation temperatures based on the most upstream thermocouple for $G = 343 \text{ kg/m}^2 \text{ s}$ and the most downstream thermocouple for $G = 970$ and $1589 \text{ kg/m}^2 \text{ s}$. Shown are both transient and steady state data to illustrate both how the steady-state boiling curve data are reached following each power increment, and the clear wall temperature excursion following the attainment of CHF. Fig. 8 shows CHF increases monotonically with increasing mass velocity.

Fig. 9(a)–(c) shows the variations of CHF with mass velocity, G , inlet quality, x_i , and exit quality, x_o , respectively. Fig. 9(a) shows the expected trend of CHF increasing with increasing mass velocity. Notice how CHF increases faster at low than at high mass velocities. This increase is far slower above $700 \text{ kg/m}^2 \text{ s}$. Fig. 9(b) and (c) shows CHF increases with increases in x_i and x_o . Despite the reduced liquid content with increasing quality, this CHF trend can be explained by the higher quality values increasing liquid velocity near the heated wall. Notice that the quality range is broader at low mass velocities. The present experimental setup precluded the attainment of high qualities for high mass velocities because of an appreciable increase in pressure drop across the flow channel.

Experiments with mass velocities below $370 \text{ kg/m}^2 \text{ s}$ show certain differences in interfacial behavior during the CHF transient from those observed at higher mass velocities. There is clear separation

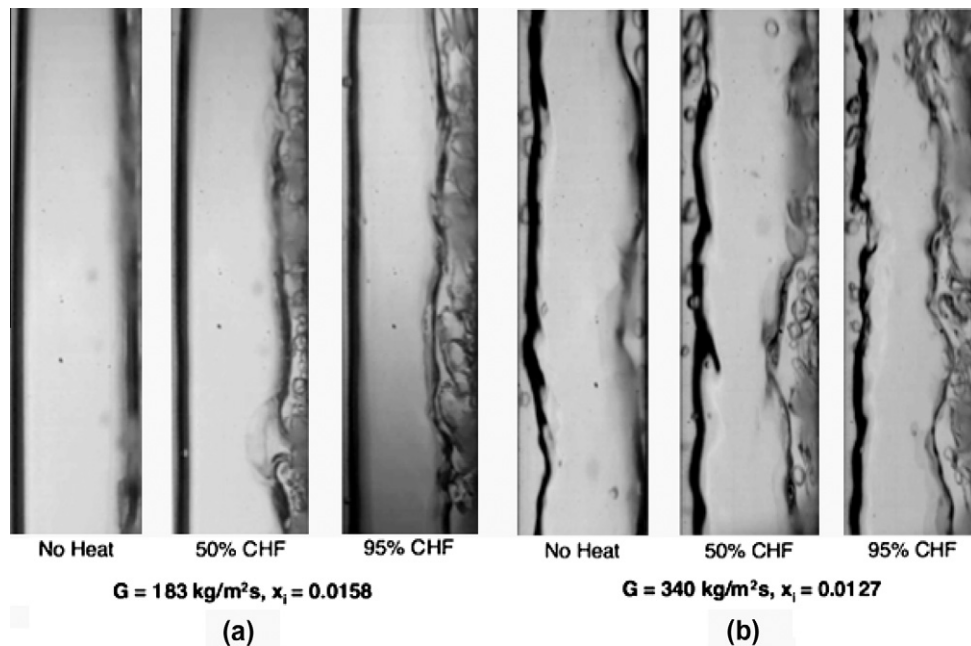


Fig. 5. Variation of flow boiling behavior in inlet region with increasing heat flux for (a) $G = 183 \text{ kg/m}^2 \text{ s}$ and $x_i = 0.0158$, and (b) $G = 340 \text{ kg/m}^2 \text{ s}$ and $x_i = 0.0127$.

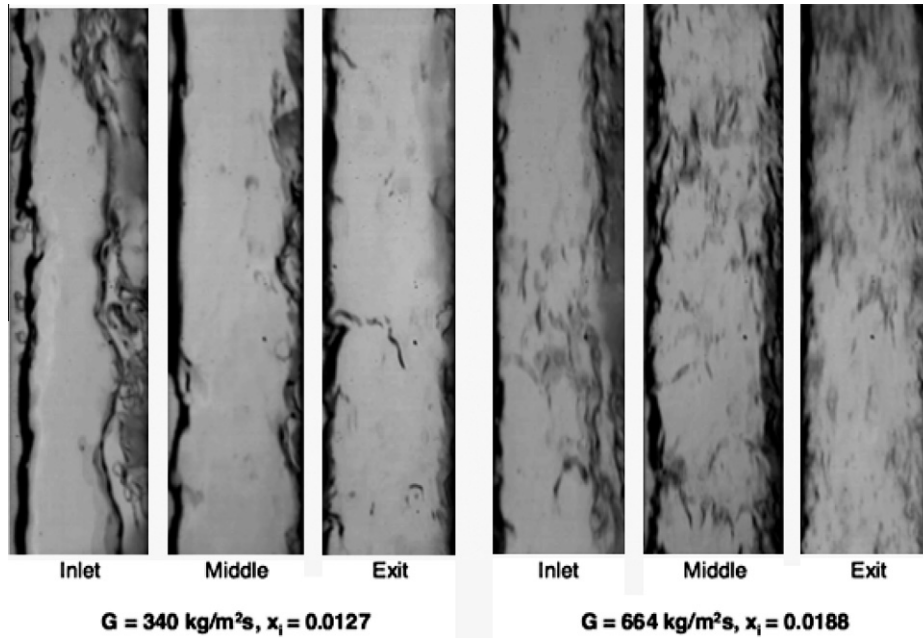


Fig. 6. Variation of flow boiling behavior at CHF- for (a) $G = 340 \text{ kg/m}^2 \text{ s}$ and $x_i = 0.0127$, and (b) $G = 664 \text{ kg/m}^2 \text{ s}$ and $x_i = 0.0188$.

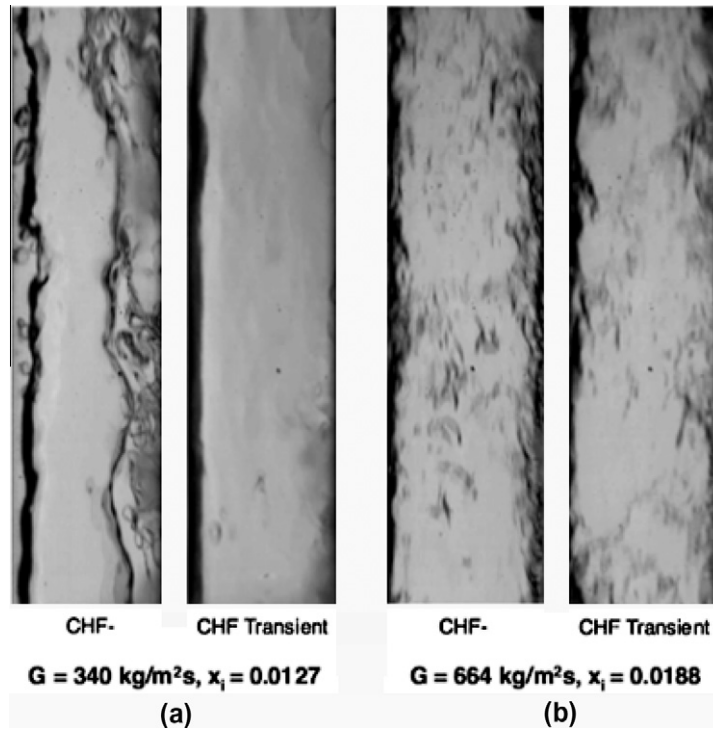


Fig. 7. Flow boiling behavior at CHF- and during CHF transient for (a) $G = 340 \text{ kg/m}^2 \text{ s}$ and $x_i = 0.0127$ in inlet region, and (b) $G = 664 \text{ kg/m}^2 \text{ s}$ and $x_i = 0.0188$ in exit region.

between the individual flow layers in the inlet region below $370 \text{ kg/m}^2 \text{ s}$, while the flow behavior is more difficult to ascertain at high mass velocities. There are also clear differences in the location of CHF occurrence along the heated wall. Fig. 10(a) and (b) shows temporal temperature records measured by the heated wall's five thermocouples during the CHF transient up to and including the instant the electrical power input to the heated wall is cut-off. In these plots, T_1 denotes the most upstream thermocouple and T_5 the most downstream. For the lower mass velocity of $G = 340.6 \text{ kg/m}^2 \text{ s}$ ($x_i = 0.0269$), Fig. 10(a) shows CHF commences first at the

location of T_1 followed by T_2 . It can clearly be seen that T_1 is also consistently higher than temperatures measured by the other thermocouples. On the other hand, Fig. 10(b) shows CHF for the high mass velocity of $G = 1589 \text{ kg/m}^2 \text{ s}$ ($x_i = 0.116$) commences first at the downstream location of T_5 followed by T_4 .

5. Separated control-volume-based model

A new separated flow model is proposed to determine the key flow variables required for CHF prediction. Fig. 11 shows a

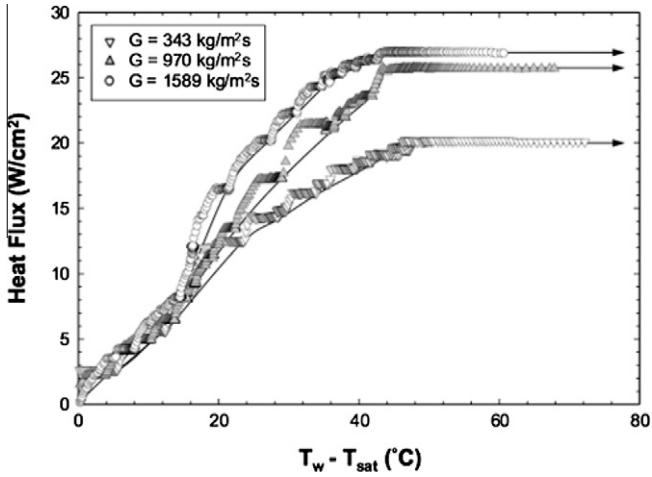


Fig. 8. Boiling curves for $G = 343 \text{ kg/m}^2 \text{ s}$ ($x_i = 0.153$), $G = 970 \text{ kg/m}^2 \text{ s}$ ($x_i = 0.084$) and $G = 1589 \text{ kg/m}^2 \text{ s}$ ($x_i = 0.081$).

schematic of vertical upflow with finite inlet vapor void based on conditions observed at CHF-. The flow upstream of the heated wall consists of a liquid layer along the walls surrounding a large central vapor core. Slip flow assumptions are adopted here, meaning each flow layer is characterized by a mean velocity while allowing for velocity differences between the different layers. Pressure is assumed uniform across the channel's cross-sectional area at each axial location. Two different cross-sections of the flow are shown in Fig. 11, one for the adiabatic flow upstream of the heated portion of the channel and the other for the heated portion.

For the adiabatic region, flow symmetry results in a uniform liquid layer thickness along all four channel walls. Momentum conservation for the vapor and liquid portions of the channel yields the following respective relations,

$$G^2 \frac{d}{dz} \left[\frac{x_i^2}{\rho_g \alpha_i} \right] = -\alpha_i \frac{dP}{dz} \mp \frac{\tau_i P_i}{A} - \rho_g \alpha_i g \tag{1}$$

and

$$G^2 \frac{d}{dz} \left[\frac{(1-x_i)^2}{\rho_f (1-\alpha_i)} \right] = -(1-\alpha_i) \frac{dP}{dz} - \frac{\tau_{wf} P_{wf}}{A} \pm \frac{\tau_i P_i}{A} - \rho_f (1-\alpha_i) g. \tag{2}$$

In the above equations, x_i is the inlet quality, α_i the inlet void fraction, P the pressure, τ_{wf} the wall shear stress for the liquid layer, τ_i the interfacial shear stress between liquid and vapor layers, A the cross-sectional area of the channel, P_{wf} the channel perimeter, and P_i the interfacial perimeter between the liquid and vapor layers. The \pm sign in the interfacial shear terms is intended to allow for any variations in the direction of the shear stress, depending on local velocity differences between the two layers.

Applying mass and energy conservation to this adiabatic cross-section yields $dx_i/dz = 0$. Property variations are neglected and Eqs. (1) and (2) are solved simultaneously to determine the void fraction at the inlet to the heated portion of the channel. An iterative procedure is adopted because the equations involve wall and interfacial shear stresses that are functions of flow velocities that, in turn, are functions of void fraction. The procedure for determining the shear stresses will be discussed later.

A third vapor layer begins to form at the leading edge of the heated wall, resulting in a separated four-layer flow as depicted

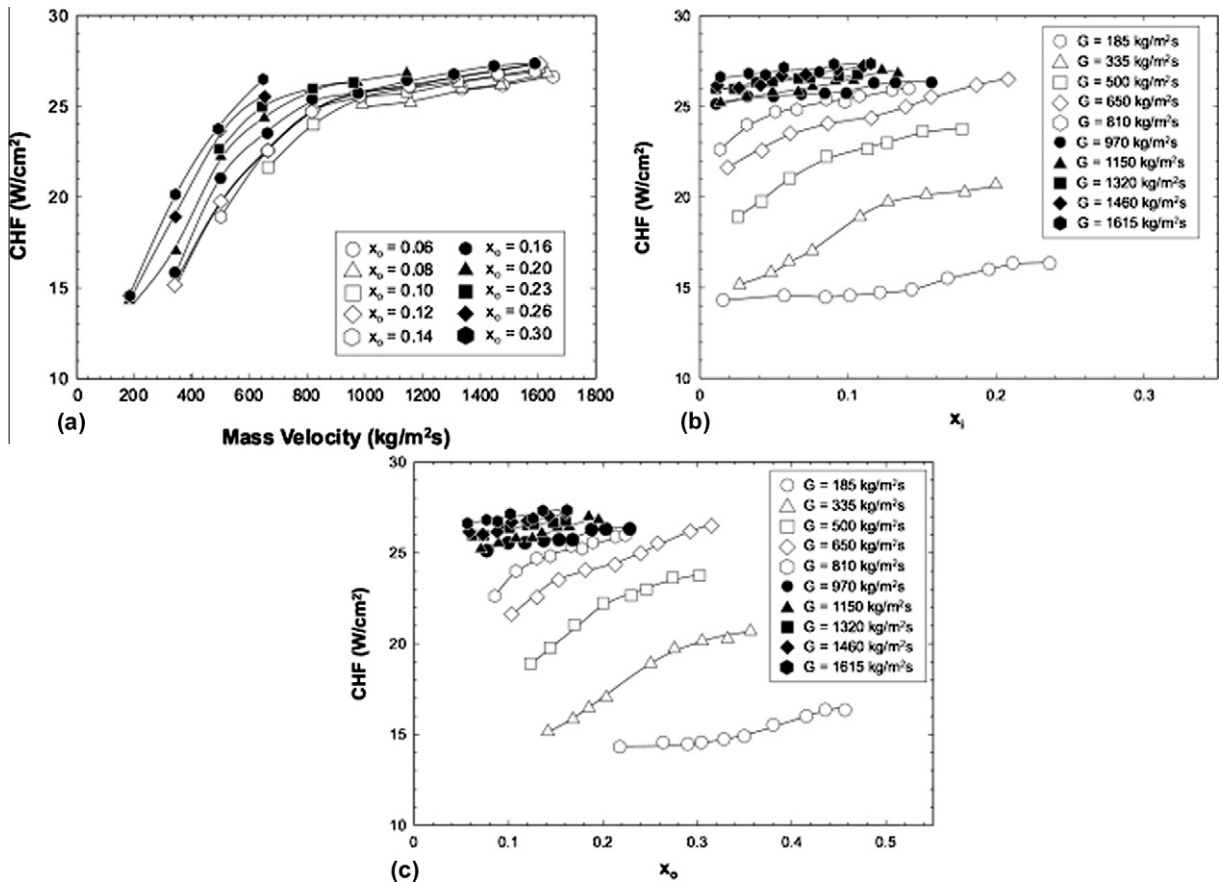


Fig. 9. Variation of CHF with (a) mass velocity, (b) inlet flow quality and (c) exit flow quality.

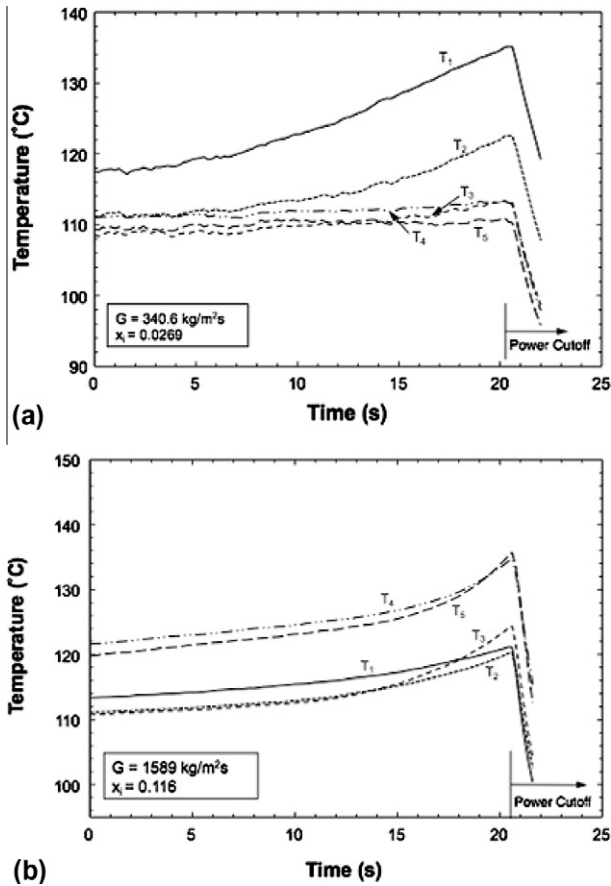


Fig. 10. Temporal records of heated wall thermocouples during CHF transient for (a) $G = 340.6 \text{ kg/m}^2 \text{ s}$ ($x_i = 0.0269$), and (b) $G = 1589 \text{ kg/m}^2 \text{ s}$ ($x_i = 0.116$).

in the top cross-section in Fig. 11. Layer 1 is comprised of liquid along the three insulated walls of the channel. Layer 2 represents

the central vapor core. Layers 3 and 4 represent the liquid and wavy vapor layers, respectively, adjacent to the heated wall. The mass flow rate of the wavy vapor layer 4 increases along the heated wall due to evaporation of liquid layer 3.

Mass, momentum and energy conservation laws are applied to a control volume of length Δz of the flow channel starting with the upstream edge of the heated wall. Because the liquid layer upstream of the heated channel is uniform in thickness, the mass flow fraction of liquid layer 1 along the insulated walls at the inlet to the heated wall can be expressed as

$$x_{f1,i} = \frac{w + 2H}{2w + 2H} (1 - x_i) \tag{3}$$

Similarly, the mass flow fraction of liquid layer 3 adjacent to the insulated walls at the inlet to the heated wall can be expressed as

$$x_{f3,i} = \frac{w}{2w + 2H} (1 - x_i) \tag{4}$$

Similar relations are adopted for area fraction of liquid along the adiabatic walls (layer 1) and adjacent to the heated wall (layer 3), respectively, at the inlet to the heated wall,

$$\varepsilon_{f1,i} = \frac{w + 2H}{2w + 2H} (1 - \alpha_i) \tag{5}$$

and

$$\varepsilon_{f3,i} = \frac{w}{2w + 2H} (1 - \alpha_i) \tag{6}$$

Another assumption that is adopted in the model is negligible heat transfer between the vapor core and all surrounding liquid, i.e., the flow quality of the vapor core is conserved and $x_2 = x_i$.

With the inlet mass and area fractions fully specified, the following equations are used to relate flow quality, velocity and area fraction for the insulated wall liquid layer (1), middle vapor core layer (2), heated wall liquid layer (3), and heated wall wavy vapor layer (4), respectively, at any axial location z along the heated portion of the channel

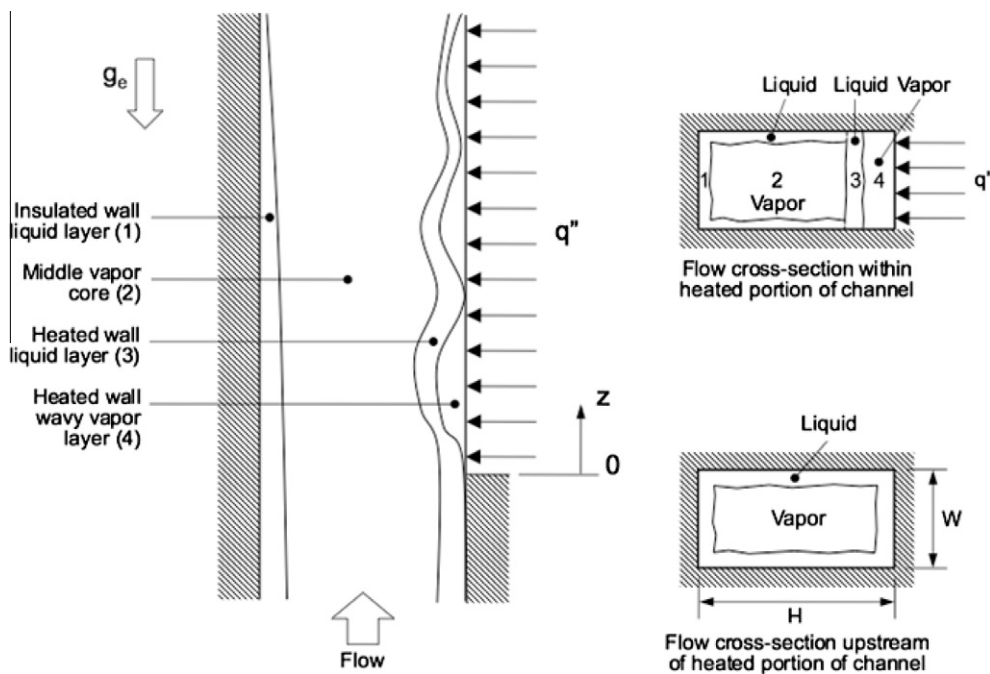


Fig. 11. Schematic of different layers in vertical channel with inlet vapor void at CHF.

$$x_{f1} = \frac{\rho_f U_{f1} A_{f1}}{GA} = \frac{\rho_f U_{f1} \varepsilon_{f1}}{G}, \quad (7)$$

$$x_2 = \frac{\rho_g U_{g2} A_{g2}}{GA} = \frac{\rho_g U_{g2} \alpha_2}{G} = x_i, \quad (8)$$

$$x_{f3} = \frac{\rho_f U_{f3} A_{f3}}{GA} = \frac{\rho_f U_{f3} (1 - \varepsilon_{f1} - \alpha_2 - \alpha_4)}{G}, \quad (9)$$

and

$$x_4 = \frac{\rho_g U_{g4} A_{g4}}{GA} = \frac{\rho_g U_{g4} \alpha_4}{G}. \quad (10)$$

Conservation of mass for the entire cross-section combined gives $dW/dz = 0$, which implies both W and G are constant. Because the entire flow is saturated, there is no temperature gradient between the four fluid layers. Therefore, it is assumed the mass flow rates of the insulated wall liquid layer ($x_{f1}W$) and central vapor core (x_2W) are both constant, which implies both x_{f1} and x_2 are constant. This also implies that $x_{f3} = x_{f3,i} - x_4$; i.e., the growth of the heated wall wavy vapor layer (4) is accounted for entirely by evaporation of the heated wall liquid layer (3). Conservation of mass yields the following relation for the rate of liquid evaporation along the interface between layers 3 and 4

$$W'_{fg} = GA \frac{dx_4}{dz}. \quad (11)$$

Applying momentum conservation to control volumes of length Δz encompassing the insulated wall liquid layer (1), central vapor core layer (2), heated wall liquid layer (3), and heated wall wavy vapor layer (4) yields, respectively,

$$G^2 \frac{d}{dz} \left[\frac{x_{f1}^2}{\rho_f \varepsilon_{f1}} \right] = -\varepsilon_{f1} \frac{dP}{dz} - \frac{\tau_{wf1} P_{wf1}}{A} \pm \frac{\tau_{i12} P_{i12}}{A} \mp \frac{\tau_{i13} P_{i13}}{A} - \rho_f \varepsilon_{f1} g, \quad (12)$$

$$G^2 \frac{d}{dz} \left[\frac{x_2^2}{\rho_g \alpha_2} \right] = -\alpha_2 \frac{dP}{dz} \mp \frac{\tau_{i12} P_{i12}}{A} \mp \frac{\tau_{i23} P_{i23}}{A} - \rho_g \alpha_2 g, \quad (13)$$

$$G^2 \frac{d}{dz} \left[\frac{x_{f3}^2}{\rho_f (1 - \varepsilon_{f1} - \alpha_2 - \alpha_4)} \right] + W'_{fg} u_{i34} = -(1 - \varepsilon_{f1} - \alpha_2 - \alpha_4) \frac{dP}{dz} - \frac{\tau_{wf3} P_{wf3}}{A} \pm \frac{\tau_{i13} P_{i13}}{A} \pm \frac{\tau_{i23} P_{i23}}{A} \pm \frac{\tau_{i34} P_{i34}}{A} - \rho_f (1 - \varepsilon_{f1} - \alpha_2 - \alpha_4) g, \quad (14)$$

and

$$G^2 \frac{d}{dz} \left[\frac{x_4^2}{\rho_g \alpha_4} \right] - W'_{fg} u_{i34} = -\alpha_4 \frac{dP}{dz} - \frac{\tau_{wg4} P_{wg4}}{A} \mp \frac{\tau_{i34} P_{i34}}{A} - \rho_g \alpha_4 g. \quad (15)$$

In the above equations, τ_{wf1} , τ_{wf3} and τ_{wg4} are the wall shear stresses for the insulated wall liquid layer, heated wall liquid layer and heated wall wavy vapor layer, respectively, τ_{i12} , τ_{i13} , τ_{i23} , and τ_{i34} the interfacial shear stresses between insulated wall liquid layer and vapor core, insulated wall liquid layer and heated wall liquid layer, vapor core and heated wall liquid layer, and heated wall liquid layer and heated wall vapor layer, respectively, P_{wf1} , P_{wg2} , P_{wf3} and P_{wg4} the perimeters of the insulated wall liquid layer, vapor core, heated wall liquid layer and heated wall wavy vapor layer, respectively, in contact with the channel walls, and P_{i12} , P_{i13} , P_{i23} and P_{i34} the contact perimeters between the insulated wall liquid layer and vapor core, insulated wall liquid layer and heated wall liquid layer, vapor core and heated wall liquid layer, and heated wall liquid layer and heated wall vapor layer, respectively. The \pm sign in

the interfacial shear terms is again intended to allow for any variations in the directions of the shear stresses, depending on local velocity differences between the four layers. The shear stress direction can be traced on a local basis from numerical solution of the momentum equations.

Because the vapor generated at the wall is ejected normal to the wall, it will have no initial stream-wise velocity [9] and, as such, does not contribute stream-wise momentum to the control volume. Therefore, the interfacial momentum terms in Eqs. (14) and (15) are neglected. The wall shear stress for each phase is defined as

$$\tau_{w,kj} = \frac{1}{2} \rho_k U_{k,j}^2 f_{kj}, \quad (16)$$

where $k = f$ or g , depending on the phase, and $j = 1-4$, depending on layer number. The friction factor in Eq. (16) is obtained from the following relation by Bhatti and Shah [29],

$$f_{kj} = C_1 + \frac{C_2}{Re_{D,kj}^{1/C_3}} = C_1 + \frac{C_2}{\left(\frac{\rho_k U_{k,j} D_{kj}}{\mu_k} \right)^{1/C_3}}, \quad (17)$$

where $C_1 = 0$, $C_2 = 16$ and $C_3 = 1$ for laminar flow ($Re_{D,kj} \leq 2100$), $C_1 = 0.0054$, $C_2 = 2.3 \times 10^{-8}$ and $C_3 = -2/3$ for transitional flow ($2100 < Re_{D,kj} \leq 4000$), and $C_1 = 0.00128$, $C_2 = 0.1143$ and $C_3 = 3.2154$ for turbulent flow ($Re_{D,kj} > 4000$). The diameter in Eq. (17) is defined as $D_{kj} = 4A_{kj}/P_{kj}$.

The four interfacial shear stresses are determined according to the relations

$$\tau_{i12} = \frac{C_{f,i}}{2} \rho_g (U_{f1} - U_{g2})^2, \quad (18)$$

$$\tau_{i23} = \frac{C_{f,i}}{2} \rho_g (U_{g2} - U_{f3})^2, \quad (19)$$

$$\tau_{i34} = \frac{C_{f,i}}{2} \rho_g (U_{f3} - U_{g4})^2, \quad (20)$$

and

$$\tau_{i13} = \frac{C_{f,i}}{2} \rho_g (U_{f1} - U_{f3})^2, \quad (21)$$

where $C_{f,i}$ is the interfacial friction coefficient. Galloway and Mudawar [8] examined several models to determine $C_{f,i}$ and recommended a constant value of 0.5 for a wavy vapor–liquid interface. This value is adopted here for interfaces between all four layers.

Applying energy conservation to a control volume of length Δz encompassing the entire cross-sectional area of the channel yields

$$\frac{dx}{dz} = \frac{dx_4}{dz} = \frac{q'' w}{Wh_{fg}}. \quad (22)$$

The model equations are solved simultaneously using a fourth-order Runge–Kutta numerical scheme along the channel using saturated properties based on local pressure. This yields values for pressure, qualities, area fractions and velocities of the four layers for every Δz axial increment from the upstream edge of the heated wall to the downstream edge. The main inputs required for the model, which are defined at the leading edge of the heated wall, are mass velocity, inlet pressure, inlet quality x_i , inlet vapor void fraction α_i , and wall heat flux q'' .

Fig. 12 shows variations of area fractions of the four layers along the heated portion of the flow channel for $G = 343.3 \text{ kg/m}^2 \text{ s}$, $P_i = 145.17 \text{ kPa}$, $x_i = 0.1082$, and $q'' = 18.70 \text{ W/cm}^2$. To obtain these results, Eqs. (1) and (2) are solved first to obtain $\alpha_i = 0.84$. The area fractions are segregated by $\varepsilon_{f1} + \alpha_2$ for the combined insulated wall liquid and vapor core, α_4 for the heated wall wavy vapor layer, and $1 - \varepsilon_{f1} - \alpha_2 - \alpha_4$ for the heated wall liquid layer. The model shows

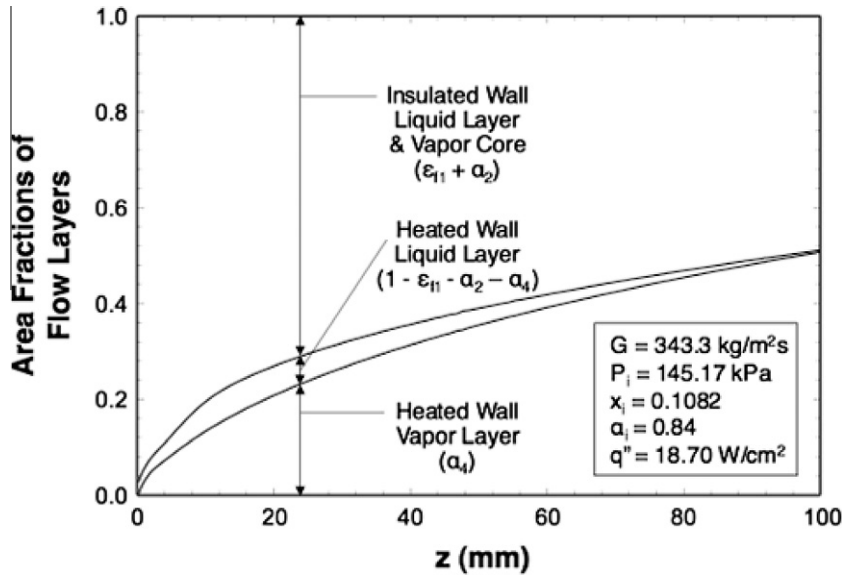


Fig. 12. Model predictions of axial variations of area fractions of different flow layers.

the heated wall wavy vapor layer growing axially in thickness, while the combined insulated wall liquid layer and vapor core are squeezed along because of the axially increasing shear stresses.

As discussed earlier, the separated four-layer behavior is recognizable mostly in the inlet region of the heated wall and lower mass velocities, but difficult to track for the middle and exit regions, especially at high mass velocities. Recall that the model tackles all the forces acting axially on the control volumes used. The model does not account for any transverse forces that can cause downstream mixing between the layers. For example, vapor effusion perpendicular to the heated wall imparts momentum that is not accounted for in the model. It can therefore be concluded that the model's greatest value is in predicting interfacial behavior in the upstream region. As shown in Fig. 10(a), this is the region where CHF is detected first for relatively low mass velocities, rendering the model especially effective at predicting CHF for these conditions. Even for high mass velocities, the Interfacial Lift-off Model is based on upstream development of the heated wall wavy vapor layer, which is where the interfacial wavelength between the liquid and vapor heated wall layers is established [9].

6. CHF predictions

The present CHF data are compared to predictions of both prior empirical correlations [30–35] and the Interfacial Lift-off Model. Table 1 provides details of three correlations that were developed for flow boiling CHF in rectangular channels and three others for circular channels. Since some of these correlations are capable of predicting both subcooled and saturated inlet conditions, the subcooling term in the correlations is set to zero when comparing predictions to the present data. Notice that some of these correlations were developed for water alone while others are applicable to other fluids as well.

Notice in Table 1 that some of previous CHF correlations are based on a partially heated circumference and others on full circumferential heating. The present rectangular channel is subjected to heating along a heated perimeter equal to one width (w) of the channel's cross-section. Therefore, the channel diameter in the correlations is substituted with the equivalent heated diameter

$$D_{h,e} = \frac{4A}{w} = 4H. \quad (23)$$

Fig. 13 compares predictions of the six correlations to the present data. The accuracy of individual correlations is ascertained using mean absolute error, which is defined as

$$MAE = \frac{1}{M} \sum \frac{|\text{CHF}_{\text{pred}} - \text{CHF}_{\text{exp}}|}{\text{CHF}_{\text{exp}}} \times 100\%. \quad (24)$$

With a MAE of 20.78%, Mishima and Ishii's correlation [32] shows the best agreement with the present data. It is followed in accuracy by Katto and Ohno's correlation [33], with a MAE of 24.78%. Despite being recommended specifically for rectangular channels, Katto's correlation [31] gave inferior predictions to those of Katto and Ohno, evidenced by a MAE of 56.18% compared to 24.78%. The Bowring correlation [30] has a moderate MAE of 42.45% but could not capture the correct dependence of CHF on mass velocity. It is followed in accuracy by the correlation of Sudo et al. [34], which has a MAE of 71.39%. With a MAE of 581.35%, the Oh and Englert's correlation [35] proved least accurate among the correlations tested. It is important to emphasize that poor predictive capability of a given correlation is not necessarily a measure of the general accuracy of the correlation, but its lack of suitability to the working fluid, flow geometry and operating conditions of the present study.

The present CHF data are also compared to predictions of the Interfacial Lift-off Model. This model was highly effective in predicting flow boiling CHF with zero inlet vapor void [7–9,15,26,27]. In the original model, the flow arrives at the heated portion of the channel in saturated or subcooled liquid state. A wavy vapor layer begins to develop along the heated wall at CHF-. The model is built on the observation that partial wetting of the wall at CHF- is possible only in wetting fronts corresponding to the troughs of the wavy vapor layer interface. CHF is triggered by lift-off of a wetting front, locally preventing liquid access to the wall. Subsequent to this lift-off, heat from the wall has to be concentrated in a fewer number of wetting fronts, which accelerates the lift-off of the remaining wetting fronts and producing the expected accelerating unsteady rise in the wall temperature.

Zhang et al. [15] showed that CHF for zero inlet subcooling can be predicted according to the following relation,

$$q''_m = b \rho_g h_{fg} \left[\left(\frac{4\pi\sigma\delta}{\rho_g b \lambda_c^2} \sin(b\pi) \right) \right]_{z_*}^{1/2}, \quad (25)$$

Table 1
Saturated flow boiling CHF correlations and corresponding MAE in predicting present CHF data.

Author(s)	Equation	Comments	MAE
Bowring [30]	$q_m'' = \frac{A + 0.25D_{h,e}G\Delta h_{sub,i}}{C + L}$ $\Delta h_{sub,i} = h_f - h_i, A = \frac{2.317(D_{h,e}Gh_{fg}/4)F_1}{1.0 + 0.0143F_2D_{h,e}^{0.5}G}$ $C = \frac{0.077F_3D_{h,e}G}{1.0 + 0.347F_4(G/1356)^n}$ $n = 2.0 - 0.5P_R, P_R = 0.145P_o, P_o \text{ in MPa}$ $F_1 = \frac{1}{1.917} \{P_R^{18.942} \exp[20.89(1.0 - P_R)] + 0.917\}$ $F_2 = \frac{1.309F_1}{P_R^{1.316} \exp[2.444(1.0 - P_R)] + 0.309}$ $F_3 = \frac{1}{1.667} \{P_R^{17.023} \exp[16.658(1.0 - P_R)] + 0.667\}$ $F_4 = F_3 P_R^{6.49}$	–Circular channel –Vertical upflow –Uniformly heated	42.45%
Katto [31]	$q_m'' = q_{m0}'' \left(1.0 + K \frac{\Delta h_{sub,i}}{h_{fg}} \right)$ $q_{m01}'' = 0.25(Gh_{fg}) \frac{1}{L/D_{h,e}}$ $q_{m02}'' = C(Gh_{fg}) We_L^{-0.043} \frac{1}{L/D_{h,e}}, We_L = \frac{G^2 L}{\sigma \rho_f}$ $q_{m03}'' = 0.15(Gh_{fg}) \left(\frac{\rho_g}{\rho_f} \right)^{0.133} We_L^{-1/3} \frac{1}{1 + 0.0077L/D_{h,e}}$ $q_{m03}'' = 0.26(Gh_{fg}) \left(\frac{\rho_g}{\rho_f} \right)^{0.133} We_L^{-0.433} \frac{(L/D_{h,e})^{0.171}}{1 + 0.0077L/D_{h,e}}$ <p>For $L/D_{h,e} < 50, C = 0.25$ For $L/D_{h,e} > 50, C = 0.34$ $K_1 = 1$ $K_2 = \frac{0.261}{CWe_L^{-0.043}}$ $K_3 = \frac{0.5556(0.0308 + D_{h,e}/L)}{(\rho_g/\rho_f)^{0.133} We_L^{-1/3}}$ When $q_{m01}'' < q_{m02}'', q_{m0}'' = q_{m01}'', K = K_1$ When $q_{m01}'' > q_{m02}'', \text{ if } q_{m02}'' < q_{m03}'', q_{m0}'' = q_{m02}'', K = K_2$ If $q_{m02}'' > q_{m03}'', \text{ if } q_{m03}'' < q_{m04}'', q_{m0}'' = q_{m03}'', K = K_3$ If $q_{m03}'' > q_{m04}'', q_{m0}'' = q_{m04}''$</p>	–Rectangular channel –Vertical flow <u>For water:</u> One-sided heated wall: $26 < L/D_{h,e} < 500$ for $P = 3.2\text{--}13.8$ MPa Two-sided heated wall: $0.417 < L/D_{h,e} < 6.02$ for $P = 101$ kPa <u>For R-113:</u> Two-sided heated walls: $L/D_{h,e} = 25$ for $P = 120\text{--}147$ kPa	56.18%
Mishima and Ishii [32]	$q_m'' = \frac{A}{A_b} h_{fg} \left[\left(\frac{1}{C_0} - 0.11 \right) \sqrt{\rho_g g (\rho_f - \rho_g) D_{h,e}} + \frac{\Delta h_{sub,i}}{h_{fg}} G \right]$ <p>For rectangular channels: $C_0 = 1.35 - 0.35 \sqrt{\frac{\rho_g}{\rho_f}}$ For round tubes: $C_0 = 1.2 - 0.2 \sqrt{\frac{\rho_g}{\rho_f}}$</p>	–Circular internally heated annulus –Vertical upflow <u>For water:</u> $D_i = 0.02045$ m $D_o = 0.02596$ m $L_h = 0.5969$ m $P = 101$ kPa $G = 0\text{--}600$ kg/m ² s $\Delta h_{sub,i} = 160\text{--}330$ kJ/kg	20.78%
Katto and Ohno [33]	$q_m'' = q_{m0}'' \left(1.0 + K \frac{\Delta h_{sub,i}}{h_{fg}} \right)$ $q_{m01}'' = C(Gh_{fg}) We_L^{-0.043} \frac{1}{L/D_{h,e}}$ $q_{m02}'' = 0.1(Gh_{fg}) \left(\frac{\rho_g}{\rho_f} \right)^{0.133} We_L^{-1/3} \frac{1}{1 + 0.0031L/D_{h,e}}$ $q_{m03}'' = 0.098(Gh_{fg}) \left(\frac{\rho_g}{\rho_f} \right)^{0.133} We_L^{-0.433} \frac{(L/D_{h,e})^{0.27}}{1 + 0.0031L/D_{h,e}}$ $q_{m04}'' = 0.0384(Gh_{fg}) \left(\frac{\rho_g}{\rho_f} \right)^{0.6} We_L^{-0.173} \frac{1}{1 + 0.28We^{-0.233}(L/D_{h,e})}$ $q_{m05}'' = 0.234(Gh_{fg}) \left(\frac{\rho_g}{\rho_f} \right)^{0.513} We_L^{-0.433} \frac{(L/D_{h,e})^{0.27}}{1 + 0.0031L/D_{h,e}}$ <p>For $L/D_{h,e} < 50, C = 0.25$ For $50 \leq L/D_{h,e} \leq 150, C = 0.25 + 0.0009(L/D_{h,e} - 50)$ For $150 < L/D_{h,e}, C = 0.34$</p>	–Circular channel –Vertical upflow –Uniformly heated <u>For water:</u> $20 < L/D_{h,e} < 500$ $P = 10\text{--}200$ bar <u>For R-12:</u> $D_{h,e} = 0.01$ m $L = 1$ m $P = 1.96\text{--}3.44$ MPa $G = 120\text{--}2100$ kg/m ² s $\Delta h_{sub,i} = 0.4\text{--}39.9$ kJ/kg	24.78%

(continued on next page)

Table 1 (continued)

Author(s)	Equation	Comments	MAE
	$K_1 = \frac{0.261}{CWe_L^{-0.043}}$ $K_2 = \frac{0.8333(0.0124 + D_{h,e}/L)}{(\rho_g/\rho_f)^{0.133}We_L^{-1/3}}$ $K_3 = \frac{1.12(1.52We_L^{-0.233} + D_{h,e}/L)}{(\rho_g/\rho_f)^{0.6}We_L^{-0.173}}$ <p>For $\rho_g/\rho_f < 0.15$:</p> <p>When $q''_{m01} < q''_{m02}$, $q''_{m0} = q''_{m01}$</p> <p>When $q''_{m01} > q''_{m02}$, if $q''_{m02} < q''_{m03}$, $q''_{m0} = q''_{m02}$;</p> <p>if $q''_{m02} > q''_{m03}$, $q''_{m0} = q''_{m03}$</p> <p>When $K_1 > K_2$, $K = K_1$; when $K_1 < K_2$, $K = K_2$</p> <p>For $\rho_g/\rho_f > 0.15$:</p> <p>When $q''_{m01} < q''_{m05}$, $q''_{m0} = q''_{m01}$</p> <p>When $q''_{m01} > q''_{m05}$, if $q''_{m05} > q''_{m04}$, $q''_{m0} = q''_{m05}$;</p> <p>if $q''_{m05} < q''_{m04}$, $q''_{m0} = q''_{m04}$</p> <p>When $K_1 > K_2$, $K = K_1$; when $K_1 < K_2$, if $K_2 < K_3$, $K = K_2$;</p> <p>if $K_2 > K_3$, $K = K_3$</p>		
Sudo et al. [34]	$q''_m = 0.005h_{fg}G^{0.611} \left[\rho_g(\rho_f - \rho_g)g \sqrt{\frac{\sigma}{(\rho_f - \rho_g)g}} \right]^{0.1945}$	–Rectangular channel –Vertical upflow –Two-sided heating For water: $L/D_{h,e} = 170$ $P = 98.1-196.1$ kPa $G = 0-600$ kg/m ² s	71.39%
Oh and Engert [35]	$q''_m = \frac{A}{P_{h,e}L} h_{fg} [0.458(1.0 + \frac{\Delta T_{sub,i}}{h_{fg}})G + 2.412 \sqrt{\lambda \rho_g g (\rho_f - \rho_g)}]$ $\lambda = \sqrt{\frac{\sigma}{(\rho_f - \rho_g)g}}$	–Rectangular channel –Vertical upflow –Uniformly heated For water: $P = 20-85$ kPa $G = 30-80$ kg/m ² s $\Delta T_{sub,i} = 5-72$ °C	581.25%

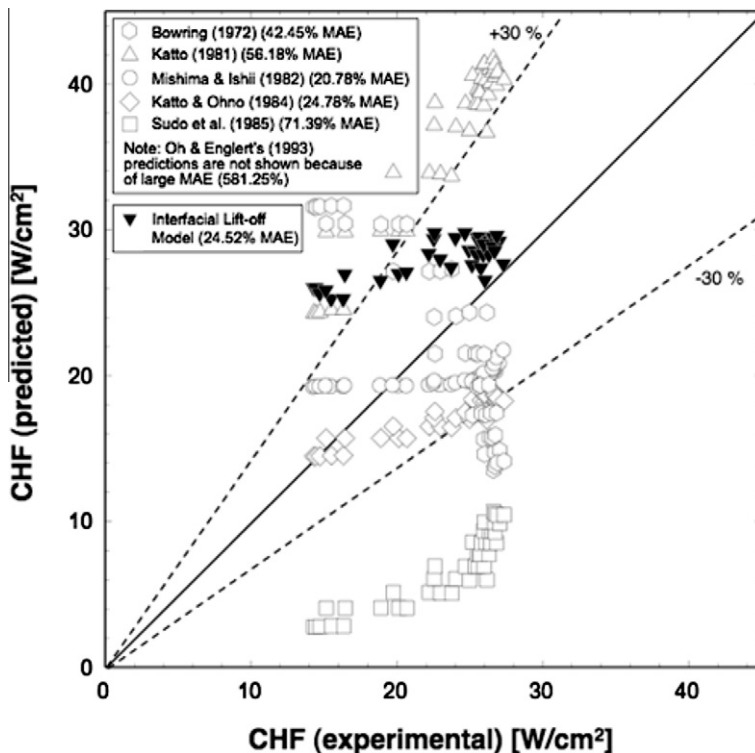


Fig. 13. Comparison of present FC-72 CHF data with predictions of prior CHF correlations and Interfacial Lift-off Model.

where $b = 0.2$, δ is the thickness of the vapor layer, and λ_c the critical wavelength of instability of the vapor layer interface. Both δ and λ_c are calculated at $z^* = z_0 + \lambda_c(z^*)$, where z_0 is the location where the velocity of the vapor layer just exceeds that of liquid. For vertical flow [15],

$$\frac{2\pi}{\lambda_c} = \frac{\rho_f'' \rho_g'' (U_g - U_f)^2}{\sigma(\rho_f'' + \rho_g'')}, \quad (26)$$

where

$$\rho_f'' = \rho_f \coth\left(\frac{2\pi}{\lambda_c} H_f\right), \quad (27)$$

and

$$\rho_g'' = \rho_g \coth\left(\frac{2\pi}{\lambda_c} H_g\right). \quad (28)$$

The terms H_f and H_g in Eqs. (27) and (28) represent the thicknesses of the liquid and vapor layers, respectively. In the original Interfacial Lift-off Model, a two-layer separated flow model is used to determine the axial variations of U_g , U_f and δ from which the values of δ and λ_c are calculated at z^* to determine CHF according to Eq. (25).

Unlike the two-layer separated flow for which the original Interfacial Lift-off Model was developed, the present study involves four separated layers. To modify the model to the conditions of the present study, the instability criterion is applied to the interface between the heated wall liquid layer and heated wall wavy vapor layer. Therefore, the vapor layer thickness, δ , is Eq. (25) is substituted by δ_4 , the vapor layer velocity, U_g , in Eq. (26) by U_{g4} , and the liquid layer velocity, U_f , in Eq. (26) by U_{f3} . The mean liquid and vapor layer thicknesses, H_f and H_g , in Eqs. (27) and (28) are given, respectively, by

$$H_f = (1 - \varepsilon_{f1} - \alpha_2 - \alpha_4)H \quad (29)$$

and

$$H_g = \alpha_4 H. \quad (30)$$

Fig. 13 shows the modified Interfacial Lift-off Model is fairly successful at predicting CHF for flow boiling in a vertical upflow channel with finite inlet vapor void, evidenced by a MAE of 24.52%. Recall that the flow visualization experiments could not provide definitive assessment of CHF for high mass velocities. Comparing the predictions of the Interfacial Lift-off Model to data corresponding to the higher mass velocities ranging from 500 to 1600 kg/m² s showed an even better MAE of 13.98%. This demonstrates the validity of this model over the entire range of mass velocities of the experimental study.

Finally, it is important to note that, while one of the CHF correlations [32] shows slightly better accuracy than the Interfacial Lift-off Model (20.78% compared to 24.52%), the model offers an entirely theoretical approach to predicting CHF.

7. Conclusions

This study explored saturated CHF for FC-72 in vertical upflow with inlet vapor void. A rectangular flow channel was used that featured an adiabatic flow development length ending with a section that was heated along one side. Both temperature measurements and high-speed video imaging methods were used to investigate the influence of inlet vapor void on interfacial behavior at heat fluxes up to CHF as well during the CHF transient. A new model was also constructed to predict CHF over a broad range of mass velocity. Following are key findings from the study.

1. The flow enters the heated portion of the channel fully separated, with a relatively thin liquid layer covering the entire perimeter of the channel surrounding a large central vapor core. At CHF-, a fairly continuous wavy vapor layer begins to develop

between the liquid layer initially covering the heated wall and the heated wall itself. This vapor layer begins evolving immediately at the leading edge of the heated wall. This results in a complex four-layer flow consisting of the liquid layer covering the insulated walls, the central vapor core, the now separated liquid layer adjacent to the heated wall, and the newly formed wavy vapor layer along the heated wall.

2. CHF increases monotonically with increases in mass velocity, inlet quality and outlet quality. The increase is more profound at low mass velocities and far slower above 700 kg/m² s.
3. Based on the flow visualization study, a new separated control-volume-based model is constructed that enables the determination of axial variations of thicknesses and mean velocities of the four layers comprising the flow at CHF-.
4. Among three popular rectangular channel and three other circular channel CHF correlations tested, the correlation by Mishima and Ishii [32], with a MAE of 20.78%, provides the best predictions of the present CHF data.
5. Incorporating the results of the new four-layer separated flow model in a modified form of the Interfacial Lift-off Model provides fairly good predictions of the CHF data over the entire range of mass velocities tested, which is evidenced by a MAE of 24.52%. Despite being slightly less accurate than the best of the correlations tested, the model offers an entirely theoretical approach to predicting CHF.

Acknowledgement

The authors are grateful for the support of the National Aeronautics and Space Administration (NASA) under Grant No. NNX09AJ51A.

References

- [1] I. Mudawar, Two-phase micro-channel heat sinks: theory, applications and limitations, in: Proceedings of the ASME/JSME 2011 8th Thermal Engineering Conference, Honolulu, HI, March 13–17, Paper No. AJTEC2011-44005, 2011.
- [2] S.S. Kutateladze, A.I. Leont'ev, Some applications of the asymptotic theory of the turbulent boundary layer, in: Proceedings of the 3rd International Heat Transfer Conference, Chicago, Illinois, vol. 3, 1966, pp. 1–6.
- [3] L.S. Tong, Boundary-layer analysis of the flow boiling crisis, Int. J. Heat Mass Transfer 11 (1968) 1208–1211.
- [4] W. Hebel, W. Detavernier, M. Decretion, A contribution to the hydrodynamics of boiling crisis in a forced flow of water, Nucl. Eng. Des. 64 (1981) 443–445.
- [5] J. Weisman, B.S. Pei, Prediction of critical heat flux in flow boiling at low qualities, Int. J. Heat Mass Transfer 26 (1983) 1463–1477.
- [6] C.H. Lee, I. Mudawar, A mechanistic critical heat flux model for subcooled flow boiling based on local bulk flow conditions, Int. J. Multiphase Flow 14 (1988) 711–728.
- [7] J.E. Galloway, I. Mudawar, CHF mechanism in flow boiling from a short heated wall – Part 1. Examination of near-wall conditions with the aid of photomicrography and high-speed video imaging, Int. J. Heat Mass Transfer 36 (1993) 2511–2526.
- [8] J.E. Galloway, I. Mudawar, CHF mechanism in flow boiling from a short heated wall – Part 2. Theoretical CHF model, Int. J. Heat Mass Transfer 36 (1993) 2527–2540.
- [9] H. Zhang, I. Mudawar, M.M. Hasan, Experimental and theoretical study of orientation effects on flow boiling CHF, Int. J. Heat Mass Transfer 45 (2002) 4463–4478.
- [10] H. Zhang, I. Mudawar, M.M. Hasan, Flow boiling CHF in microgravity, Int. J. Heat Mass Transfer 48 (2005) 3107–3118.
- [11] H. Zhang, I. Mudawar, M.M. Hasan, Assessment of dimensionless CHF correlations for subcooled flow boiling in microgravity and reduced gravity, Int. J. Heat Mass Transfer 50 (2007) 4568–4580.
- [12] D.D. Hall, I. Mudawar, Critical heat flux (CHF) for water flow in tubes – I. Compilation and assessment of world CHF data, Int. J. Heat Mass Transfer 43 (2000) 2573–2604.
- [13] D.D. Hall, I. Mudawar, Critical heat flux (CHF) for water flow in tubes – II. Subcooled CHF correlations, Int. J. Heat Mass Transfer 43 (2000) 2605–2640.
- [14] D.D. Hall, I. Mudawar, Ultra-high critical heat flux (CHF) for subcooled water flow boiling – II. High-CHF database and design equations, Int. J. Heat Mass Transfer 42 (1999) 1429–1456.
- [15] H. Zhang, I. Mudawar, M.M. Hasan, CHF model for subcooled flow boiling in Earth gravity and microgravity, Int. J. Heat Mass Transfer 50 (2007) 4039–4051.
- [16] G. Wallis, One-dimensional Two-phase Flow, McGraw-Hill, New York, 1969.

- [17] J.G. Collier, J.R. Thome, *Convective Boiling and Condensation*, third ed., Clarendon Press, Oxford, UK, 1994.
- [18] R.W. Lockhart, R.C. Martinelli, Proposed correlation of data for isothermal two-phase two-component flow in pipes, *Chem. Eng. Prog.* 45 (1949) 39–48.
- [19] R.C. Martinelli, D.B. Nelson, Prediction of pressure drop during forced circulation boiling of water, *Trans. ASME* 70 (1948) 695–702.
- [20] J.R.S. Thom, Prediction of pressure drop during forced circulation boiling of water, *Int. J. Heat Mass Transfer* 7 (1964) 709–724.
- [21] C.J. Baroczi, A systematic correlation for two-phase pressure drop, in: Eighth National Heat Transfer Conference, AIChE Paper No. 37, Los Angeles, CA, 1965.
- [22] D. Chisholm, A theoretical basis for the Lockhart–Martinelli correlation for two-phase flow, *Int. J. Heat Mass Transfer* 10 (1967) 1767–1778.
- [23] L. Friedel, Improved friction pressure drop correlations for horizontal and vertical two-phase pipe flow, in: Proceedings of the European Two-Phase Flow Group Meeting, Paper E2, Ispra, Italy, 1979.
- [24] C.O. Gersey, I. Mudawar, Effects of heater length and orientation on the trigger mechanism for near-saturated flow boiling critical heat flux – I. Photographic study and statistical characterization of the near-wall interfacial features, *Int. J. Heat Mass Transfer* 38 (1995) 629–641.
- [25] C.O. Gersey, I. Mudawar, Effects of heater length and orientation on the trigger mechanism for near-saturated flow boiling critical heat flux – II. Critical heat flux model, *Int. J. Heat Mass Transfer* 38 (1995) 643–654.
- [26] J.C. Sturgis, I. Mudawar, Critical heat flux in a long, rectangular channel subjected to onesided heating – I. Flow visualization, *Int. J. Heat Mass Transfer* 42 (1999) 1835–1847.
- [27] J.C. Sturgis, I. Mudawar, Critical heat flux in a long, rectangular channel subjected to onesided heating – II. Analysis of critical heat flux data, *Int. J. Heat Mass Transfer* 42 (1999) 1849–1862.
- [28] C.R. Kharangate, I. Mudawar, M.H. Hasan, Photographic study and modeling of critical heat flux in horizontal flow boiling with inlet vapor void, *Int. J. Heat Mass Transfer*, in review.
- [29] M.S. Bhatti, R.K. Shah, Turbulent and transitional convective heat transfer in ducts, in: S. Kakac, R.K. Shah, W. Aung, (Eds.), *Handbook of Single-phase Convective Heat Transfer*, John Wiley and Sons, New York.
- [30] R.W. Bowring, A simple but accurate round tube uniform heat flux, dryout correlation over the pressure range 0.7–17 MN/m² (100–2500 psia), AEEW-R 789, United Kingdom Atomic Energy Authority, 1972.
- [31] Y. Katto, General features of CHF of forced convection boiling in uniformly heated rectangular channels, *Int. J. Heat Mass Transfer* 24 (1981) 1413–1419.
- [32] K. Mishima, M. Ishii, Critical heat flux experiments under low flow conditions in a vertical annulus, ANL-82-6, NUREG/CR-2647, 1982.
- [33] Y. Katto, H. Ohno, An improved version of the generalized correlation of critical heat flux for the forced convective boiling in uniformly heated vertical tubes, *Int. J. Heat Mass Transfer* 27 (1984) 1641–1648.
- [34] Y. Sudo, K. Miyata, H. Ikawa, M. Kaminaga, M. Ohkawara, Experimental study of differences in DNB heat flux between upflow and downflow in vertical rectangular channel, *J. Nucl. Sci. Technol.* 22 (1985) 604–618.
- [35] C.H. Oh, S.B. Englert, Critical heat flux for low flow boiling in vertical uniformly heated thin rectangular channels, *Int. J. Heat Mass Transfer* 36 (1993) 325–335.